CONF-840910--3

UCRL-90412
PREPRINT

THEORETICAL STUDIES IN TANDEM MIRROR PHYSICS

R.H. Cohen, S.P. Auerbach, D.E. Baldwin, I.B. Bernstein, J.A. Byers, Y.-J. Chen, B.I. Cohen, R.P. Freis, J.M. Gilmore, J.H. Hammer, T.B. Kaiser, L.L. LoDestro, B. McNamara, Y. Matsuda, W.A. Newcomb, W.M. Nevins, L.D. Pearlstein, M.W. Phillips, T.D. Rognlien, J.W. Shearer G.R. Smith, J.J. Stewart

This paper was prepared for submittal to the
IAEA 10th International Conference on Plasma Physics and Controlled Nuclear Fusion Research
London, England, Sept. 12-19, 1984

July 17, 1984

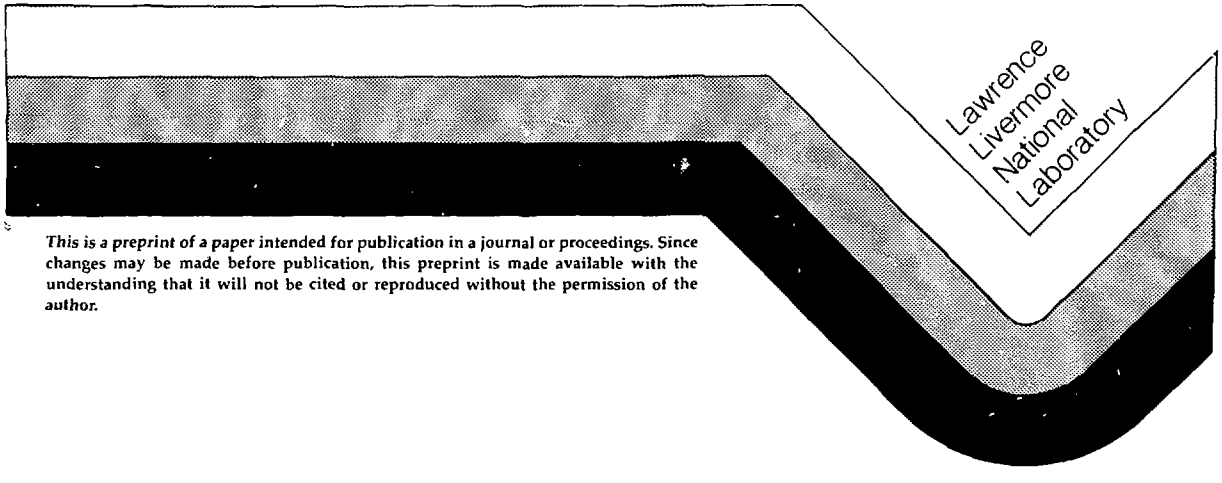

INTERNATIONAL ATOMIC ENERGY AGENCY

TENTH INTERNATIONAL CONFERENCE ON PLASMA PHYSICS AND CONTROLLED NUCLEAR FUSION RESEARCH

London, UK, 12–19 September 1984

IAEA-CN-44/ C-1-5

THEORETICAL STUDIES IN TANDEM MIRROR PHYSICS*

R.H. COHEN, S.P. AUERBACH, D.E. BALDWIN, J.A. BYERS, Y.-J. CHEN, B.I. COHEN, R.P. FREIS, J.M. GILMORE, J.H. HAMMER, T.B. KAISER, L.L. LODESTRO, B. MCNAMARA, Y. MATSUDA, W.A. NEWCOMB, W.M. NEVINS, L.D. PEARLSTEIN, T.D. ROGNLIEN, J.W. SHEARER, G.R. SMITH, and J.J. STEWART
Lawrence Livermore National Laboratory,
University of California
Livermore, California 94550, USA

I.B. BERNSTEIN
Yale University,
New Haven, Connecticut

M. W. PHILLIPS
Grumman Aerospace Corporation,
Princeton, New Jersey

*Work performed under the auspices of the U.S. Department of Energy by the Lawrence Livermore National Laboratory under contract number W-7405-ENG-48.

Abstract

THEORETICAL STUDIES IN TANDEM MIRROR PHYSICS

Recent developments in six areas of tandem-mirror theory are explored. Specifically, FLR terms (including electric-field drift) have been added to our 3-D paraxial MHD equilibrium code. Our low-frequency MHD stability analysis with FLR, which previously included only $m_\theta = 1$ rigid perturbations, has been extended to incorporate moderate m_θ, rotational drive, finite-beta effects on wall stabilization, and the well-digging effect of energetic electrons by using three computational techniques. In addition, we have examined the microstability of relativistic electrons with a loss-cone distribution, emphasizing the whistler and cyclotron-maser instabilities. We have also studied techniques for controlling radial transport, including the floating of segmented end plates and the tuning of transition-region coils, and have quantified the residual transport in a tandem mirror with axisymmetric throttle coils. Earlier work on the effect of ECRH on potentials in thermal-barrier cells has been extended. The transition between the weak- and strong-heating regimes has been examined using Fokker-Planck and Monte Carlo codes; an analytic model for the potentials relative to the end wall has been developed. Finally, our investigation of drift-frequency pumping of thermal-barrier ions has demonstrated that pumping is optimized when the magnetic fluctuation is perpendicular to both the unperturbed field and the thin fan, and that an adequate pumping rate is obtainable in future machines.

1. INTRODUCTION

In this paper we report on the status of recent developments in six areas of tandem mirror theory: magneto-hydrodynamic (MHD) equilibrium and stability, electron microstability, ion radial transport, electron-cyclotron resonant heating (ECRH), and drift pumping.

2. MAGNETOHYDRODYNAMIC EQUILIBRIUM AND STABILITY

2.1 MHD Equilibrium

In quadrupole tandem mirrors, field lines are nearly paraxial and thus MHD equilibrium equations are obtained by keeping leading-order corrections to an axisymmetric magnetic field. Similarly, FLR effects can also be computed as the

leading-order correction to the same axisymmetric field. Because both corrections are second-order in their respective smallness parameters, they enter additively. Thus, by combining results from Ref. [1], we can construct the energy:

$$U = 1/2 \int \frac{dz}{B} \, d\psi d\theta \left\{ Q \, \underset{\sim}{x}_z^2 + Y \, \underset{\sim}{x}_\theta^2 \right\} , \tag{1}$$

where $Q = B^2 + p - p_{||}$ ($Y = -\rho\omega_M\omega_{GC}$) are the MHD(FLR) stresses, respectively, and $\omega_M(\omega_{GC})$ are the macroscopic and mean guiding-center frequency, respectively. The latter expression takes this simple form for an isothermal Maxwellian plasma. In Eq. (1), $\underset{\sim}{x} = (x,y)$ is the position of the field line and the subscripts refer to partials. The first variation of U, subject to the Jacobian constraint $1 - [x,y]B = 0$, produces the current balance equation:

$$B \frac{\partial}{\partial z} \frac{iQ}{B^2} - = \left[\frac{\partial Q}{\partial \psi} (x_\theta x_{zz} + y_\theta y_{zz}) + B \frac{\partial}{\partial \theta} \frac{i_{FLR} Y}{B^2} + \frac{\partial Y}{\partial \psi} (x_\theta x_{\theta\theta} + y_\theta y_{\theta\theta}) \right] , \tag{2}$$

where the parallel current per unit flux is

$$i = B[(x_z,x) + (y_z,y)] = B[x_{z\psi}x_\theta - x_{z\theta}x_\psi + (x \to y)] , \tag{3a}$$

and, analogously,

$$i_{FLR} = B([x_\theta,x] + [y_\theta,y]) . \tag{3b}$$

These equations--in addition to the lowest-order perpendicular pressure balance ($2p_\perp + B^2 = B_V^2$), parallel pressure balance, and the boundary conditions--determine the equilibrium. Both Q and Y must be positive for well-posed equilibrium.

The numerical procedure [2] is to assume isorrhopic pressure profiles $p(\psi,B)$, determine mod-B from the perpendicular pressure balance, and then analytically solve the Jacobian constraint to obtain an initial choice for the field-line trajectories. Subsequent motion of the field lines is incompressible ($d\underset{\sim}{x}/dt = \underset{\sim}{\nabla}\phi \times \hat{z}$), and so Eq. (2) is linearized and integrated over z to generate an equation for $(B\phi)_z$. We solve, with Fourier transforms to eliminate aliases and to resolve θ-derivatives, and obtain:

$$\phi(\psi,\theta,z) = \frac{1}{B} \left[\int_o^z dz (B\theta)_z + \Lambda(\psi,\theta) \right] . \tag{4}$$

The remaining function (Λ) is determined from the constraint

that the line integral of the right side of Eq. (2) must vanish, producing an elliptic equation that is singular on the plasma boundary; note that at intermediate stages of this iterative procedure the parallel current does not vanish at the ends. The field lines are moved and the linearization is repeated until Eq. (2) is satisfied, the constraint vanishes, and the parallel current at the ends is equal to zero. It should be pointed out that only $\hat{A}$ determines the motion of the flux surface at the midplane, which is predominately an octupole motion.

For this study we assume that there is no radial electric field, consequently $Y = -\rho\omega_{*i}\langle\omega_{\nabla B}\rangle$, and because $\omega_{\nabla B} = 0(\beta)$, the FLR term is peaked on axis away from the plasma boundary. Thus, we find that the octupole distortion of the flux surface is limited more to the plasma surface when the FLR terms are included. This is shown in Fig. 1 where we compare the octupole moment of the flux surfaces for the Tandem Mirror Experiment-Upgrade (TMX-U) and the Mirror Fusion Test Facility (MFTF-B). In this study there are 10 Larmor radii in the radial scale length, and the betas of the figure caption are peak values. The average beta is 44% of the peak. With FLR the overall distortion is smaller, the parallel currents flowing through the central cell are reduced, and the axisymmetry of the central cell is better preserved. Note that the relative octupole distortion in MFTF-B is significantly lower than in TMX-U, which was a design goal.

2.2 MHD Stability

In three significant computational efforts, the low-frequency MHD stability of both quadrupole and axisymmetric tandem mirrors has been examined using standard FLR theory [1], which combines paraxial and FLR expansions. The ballooning, interchange, and rotational stability of TMX-U, MFTF-B, the Mirror Advanced Reactor Study (MARS), Phaedrus, TARA, and proposed axisymmetric configurations has been addressed. These studies have defined beta limits and determined the requirements on magnetic curvature, plasma pressure, and ambipolar potential profiles for stability.

The MHD stability studies using the TEBASCO code [3] generally are limited to the rigid ($m_\theta = 1$) displacement because it has been shown that, in the absence of E x B rotation, FLR terms stabilized all but the lowest mode numbers [4]. Recently the theory of other low-mode numbers, including rotation, has been added. This theory assumes that the lowest radial mode for a given m_θ dominates--again a consequence of FLR. However, these studies are limited to sharp-boundary pressure profiles, a valid approximation because the modes examined are global. In addition, the ballooning equation for a rigid displacement has been modified to include an improved wall representation and diamagnetic effects; the latter

introduces an important stabilizing term pointed out by Berk [5]. These two additions lead to higher central cell beta values on the stability boundary in TMX-U as well as in MFTF-B.

We have also initiated studies of wall stabilization in axisymmetric configurations to verify the stability criterion $\beta L_B^2/L_p^2 > 1$, where the subscripts refer to vacuum mod-B and the plasma scale lengths, respectively [5]. Typical results are shown in Fig. 2 where stability can be achieved for sufficiently high betas. Stability at lower beta requires shorter plasmas. However, we expect that adiabaticity and/or anisotropy-driven modes may severely limit the possible parameter ranges for wall-stabilized axisymmetric mirrors.

The stability analysis of quadrupole tandems with FLR effects has also been addressed with a three-dimensional eigenvalue code. The associated Euler-Lagrange equations are solved using a Galerkin approach to determine the spectrum of complex-valued eigenfrequencies at low and moderate m_θ. However, there is no restriction on the form of the radial trial functions to allow the rigid approximation presumed in TEBASCO to be checked.

Growth rates and stability boundaries for ballooning, interchange, and rotational modes in the low-beta TARA and Phaedrus configurations have been calculated. These results verify the strong stabilizing effect of FLR on curvature-driven ballooning modes: FLR indeed forces the mode to be rigid. As the FLR decreases, the mode becomes non-rigid and the coupling of higher angular components induced by the quadrupole coils becomes important. The $m_\theta = 1$ rigid mode is stable for the TARA and Phaedrus parameters, but the $m_\theta = 2$, $n = 0$ rotational mode is predicted to be most unstable. There is some corroborative evidence of this in Phaedrus experimental data (unpublished).

The FLORA MHD/FLR initial-value stability code integrates the Euler-Lagrange equations for the displacement of the magnetic field line using finite differences in (ψ,z,t) and Fourier analyzing in θ. We determine the MHD stability of a finite-beta, paraxial, axisymmetric equilibrium without restriction on the mode structure. In fact, a rigid, energetic electron ring can be located in the anchor cells of the tandem to provide a stabilizing magnetic well [6]. Electron-ring-stabilized, generic, axisymmetric, tandem-mirror configurations have yielded a central cell beta as large as 70%. Finally, we employed FLORA to study rotational modes with axial or radial shear in the equilibrium E x B rotation profile. For $m_\theta = 1$ and large FLR, FLORA verifies the rigid mode behavior postulated in TEBASCO.

3. ELECTRON MICROSTABILITY

We study the linear stability of waves with frequency comparable to the electron-cyclotron frequency. The modes have

a zero perpendicular wave number, and the plasmas are described by a loss-cone distribution f of relativistic electrons. In terms of the kinetic energy E and the pitch angle ϕ, we take $f = F(E)G(\phi)$ with $G(\phi) = 1$ for $\theta < \phi < \pi - \theta$ and zero otherwise, to allow analytic evaluation of one of the velocity-space integrals that appear in the dispersion relation for any F(E).

For the whistler instability, we agree with previous authors [7,8] that relativistic effects weaken the instability at mean electron energies $E > 0.1\ mc^2$. Realistic parameter regimes exist for which spatial growth of whistler modes are negligible in TMX-U and MFTF-B.

After determining that the cyclotron-maser instability is sensitive to the shape of the energy distribution F(E), we contrast results obtained with $F_1(E)$, which approximates a step function (F_1 = const at low E, zero at high E), to those with the Maxwellian $F_2(E) \propto \exp(-aE)$. Figure 3 shows the temporal growth rate ω_i, normalized to the rest-mass cyclotron frequency Ω, as a function of ω_p^2/Ω^2 for F_1 (solid curve) and F_2 (dashed curve). Note that F_1 yields much higher growth rates, a higher maximum density, and a very low minimum density. Also, we find that the stabilizing effect of cold plasma is much stronger for distribution F_2 than for F_1.

4. ION RADIAL TRANSPORT

We examine two techniques for actively controlling ion *radial transport*: adjustment of transition-region coils to minimize the radial step and floating segmented end plates to control the electric field. In a tandem mirror with axisymmetric throttle coils separating the axisymmetric solenoid from the quadrupolar transition regions, solenoid ions fall down sizable magnetic and potential hills before entering the transition regions; consequently, these ions have $v_{||} \approx v \approx$ const. We find the radial step per bounce Δr varies as $\Delta r \propto \sin 2\theta_{tp} \int dz\, \hat{\kappa}(z) \cos 2\delta\theta(z)$, where $\theta(z) = \theta_{tp} +(-)\, \delta\theta(z)$ is the azimuthal angle of an outgoing (incoming) ion, θ_{tp} is θ at the turning point, and $\hat{\kappa} \sin 2\theta$ is the geodesic curvature.

Although MFTF-B was designed to have $\int \hat{\kappa}\, dz \sim 0$ so that Δr is near zero if the azimuthal drift in the transition regions is negligible, azimuthal drifts defeat this cancellation and lead to unacceptably large, stochastic (overlapping drift-bounce resonances) radial transport for the MFTF-B parameters. The above expression for Δr suggests resetting the transition coils to make $\int dz\, \hat{\kappa} \cos 2\delta\theta = 0$. This retuning will depend on the self-consistent radial electric field E_r.

Another approach to transport control is to electrically insulate the field line ends. This forces end loss, and therefore radial loss, to be ambipolar. In current designs that have small electron diffusion coefficients, radial ion losses are reduced: readjustment of E_r leads to lower

mobility, smaller $\int dz\, \hat{\kappa} \cos 2\delta\theta$, and fewer resonant particles experiencing quadrupole fields.

In TMX-U, insulated field-line ends are approximated by segmented, floating end plates. In our study of these plates using the radial transport code TMT, the effect of field-line errors is modeled as a finite conductance between adjacent plates proportional to the fractional magnetic flux connecting them. We simulate TMX-U with two and four concentric end-plate segments using resonant-plateau ion-radial-transport coefficients. In the ideal case (no field-line errors) with two segments, the ion-particle confinement time in the central-cell-core plasma is a factor of 1.6 larger when the plates are floating than when they are grounded. Field-line errors reduce this factor to about 1.3. We note that these factors are comparable to the experimental values [9]. When four segments are used, the factors are slightly larger (1.7 and 1.5, respectively).

Assuming that these control techniques are sufficiently successful to avoid stochasticity in MFTF-B, the dominant contribution to transport comes from a boundary layer separating particles trapped in the solenoid from those passing to the nonaxisymmetric cells. A drift-kinetic analysis gives the particle diffusion coefficient: $D \simeq 0.39\, a^2\, (\nu_{th} u_s / RL)^{1/2}$, where $a \equiv \Delta r / \sin 2\theta_{tp}$, ν_{th} is the ion pitch-angle scattering rate at speed $v = v_{th} \equiv (2T/m)^{1/2}$, R is the mirror ratio from the solenoid to the peak of the axisymmetric throttle, $u_s \equiv v_{th}(1-R^{-1})^{1/2}$, and L is the solenoid length. The implied radial lifetime for MFTF-B with zero radial electric field in the transition region is about 0.4 s.

5. ELECTRON-CYCLOTRON RESONANT HEATING

Electron-cyclotron resonant heating (ECRH) is used in the thermal-barrier region of tandem mirrors to enhance the ion-confining, or plug, electrostatic potential. We have studied this process both analytically and numerically, using both a multi-region Fokker-Planck code and a Monte Carlo code. Recent calculations [10,11] show a more favorable scaling of plug-to-barrier potential Φ_{pb} when ECRH dominates collisional diffusion than in the opposite (weak ECRH) limit. When strong ECRH takes place at both the thermal barrier and the end plug but the diffusion at the barrier is stronger than at the plug, the following relation is obtained:

$$\Phi_{pb} = T_s \left(\frac{3}{4} \sqrt{\pi}\, \frac{R_{pb}^{-1}}{R_{pb}}\, \frac{n_p}{n_m}\, \exp \hat{\epsilon} \right)^{2/3} , \qquad (5)$$

where T_s is the solenoid electron temperature; R_{pb} is the plug-to-barrier mirror ratio; n_p is the plug density; $n_m = n_s \exp(-e\Phi_{sb}/T_s)$; n_s is the solenoid density; $\Phi_{sb} \equiv \Phi_s - \Phi_b$ (where Φ_s and Φ_b are the potentials

of the solenoid and barrier relative to the end wall), $\epsilon = e\Phi_{sb}/[T_s/(R_{mb}-1)]$; and R_{mb} is the mirror ratio from the solenoid mirror throat to the barrier.

The power law relation between Φ_{pb} and n_p replaces the logarithmic relation [12] valid for weak ECRH. The numerical solutions to the Fokker-Planck equation show (Fig. 4) the transition between Eq. (5) and the weak ECRH limit as the level of ECRH is varied. The ECRH power found at this transition agrees with the analytic estimate [10]. Therefore, the strong ECRH limit should be accessible for power levels available in TMX-U.

In early experiments on TMX-U at low end-cell density ($n \sim 5\times10^{11}$ cm^{-3}) and even lower solenoid density, a large plasma potential ($\sim$1 keV) resulted when the plug ECRH was applied. We ascribe this potential rise to the increased loss caused by plug electrons diffusing rapidly along their ECRH characteristics. At higher energy, these characteristics come closer together, and a small-angle scattering places electrons on characteristics intersecting the loss region, causing immediate loss. A physics model of this phenomenon illustrates the predicted loss rate $\nu_e = \nu_p(\Phi_s) + \tau_{rf}^{-1}(\Phi_b)$, where ν_p is the Pastukhov [13] loss rate and $\tau_{rf} \simeq \tau_{ee}\,\Phi_b/2E_h$. Here τ_{ee} is the electron angle-scattering rate and E_h is the hot electron energy. When equating ν_e to the ion loss rate, potentials of the order of 1 keV are obtained.

6. DRIFT PUMPING

Drift pumping is the use of RF fields to remove potential-trapped ions by transporting them radially to the plasma halo where they are lost by axial flow and/or by increasing their parallel energy so that they are no longer trapped. Both heating and transport require that the RF field resonate with one of the natural frequencies of ion motion. To preserve the ion magnetic moment, the axial bounce frequency ω_b or the drift frequency ω_d is preferred.

We identify the resonant frequencies as $\omega = k\omega_b \pm m\omega_d$; $k,m = 0,1,2\ldots$ for two RF field configurations--one with the magnetic fluctuations perpendicular ($B_\perp$) and the other parallel ($B_\parallel$) to the unperturbed field. For a simplified $B_\perp$ model, we have derived analytically and verified numerically the requirement of resonance overlap for producing stochasticity. In general, stochasticity depends on the frequency spectrum and amplitude of the applied field in combination with properties of ion motion in the equilibrium field. For $m = 1$ and $B_\perp$, the diffusion coefficient is optimum when $B_\perp$ is perpendicular to the thin fan, then scaling as $D \approx [\kappa_y B_\perp (2W_\parallel + W_\perp)]^2/\Delta\omega$, where κ_y is the curvature normal to the thin fan and $\Delta\omega$ is the bandwidth of the RF field. The resulting pumping rate is marginal for TMX-U but safe for MFTF-B and MARS.

Unless $B_{||}$ can excite a parallel electric field, it appears that $B_{||}$ is less effective than $B_{\perp}$. There are advantages of applying the RF field at the drift frequency resonance; i.e., $k = 0$: (1) unwanted trapping can be induced by breaking the axial bounce invariant $J = \int ds\, v_{||}$ by the ω_b resonance, and (2) pumping impurities can be accomplished if the drift is predominantly electric field drift.

REFERENCES

[1] NEWCOMB, W.A., Ann. Phys. **81**, (1973) 231 and J. Plasma Phys. **26** (1981) 529. The form most suitable for quadrupole geometry is best obtained from these papers.

[2] MCNAMARA, B., presented at U.S.-Japan Third Workshop on 3-D Simulation, Oakridge National Laboratory, Oakridge, TN, 1984, published by Lawrence Livermore National Laboratory, Livermore, CA, as Report UCRL-90437 (1984).

[3] BULMER, R.H., KAISER, T.B., NEVINS, W.M., NEWCOMB, W.A., PEARLSTEIN, L.D., STRAUSS, H.R., WOLLMAN, S., and WAKATANI, M., Proc. 9th Intl. Conf. Plasma Phys. Controlled Nucl. Fusion Res. (Baltimore, MD, 1982) IAEA, Vol. 1, p. 531.

[4] NEVINS, W.M., BALDWIN, D.E., KAISER, T.B., and PEARLSTEIN, L.D., Proc. Annual Controlled Theory Conf. (Austin, Texas, 1981) paper 3A1.

[5] BERK, H.L., Proc. Annual Controlled Fusion Theory Conf. (Incline Village, Nevada, 1984) paper 1B1.

[6] D'IPPOLITO, D.A., MYRA, J.R., and OGDEN, J.M., Plasma Phys. **24** (1982) 707.

[7] GLADD, N.T., Phys. Fluids **26** (1983) 974.

[8] TSANG, K.T., Phys. Fluids **27** (1984); to be published.

[9] HOOPER, E.B., BALDWIN, D.E., FOWLER, T.K., KANE, R.J., and TURNER, W.C., Lawrence Livermore National Laboratory, Livermore, CA, Report UCRL-90639 (1984); to be published in Phys. Fluids.

[10] COHEN, R.H., Phys. Fluids **26** (1983) 2774.

[11] MATSUDA, Y., and ROGNLIEN, T.D., Phys. Fluids **26** (1983) 2778.

[12] COHEN, R.H., BERNSTEIN, I.B., DORNING, J.J., and ROWLANDS, G., Nucl. Fusion **20** (1980) 1421.

[13] PASTUKHOV, V.P., Nucl. Fusion **14** (1974) 3; COHEN, R.H., RENSINK, M.E., CUTLER, T.A., MIRIN, A.A., Nucl. Fusion **18** (1978) 1229; NAJMABADI, C., CONN, R.W., COHEN, R.H., Nucl. Fusion **24** (1984) 75.

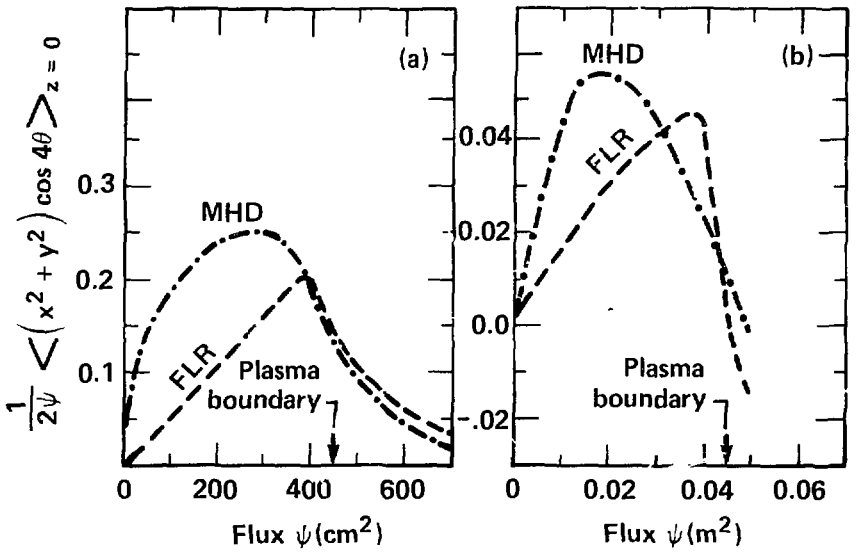

FIG. 1. Octupole moment of the flux surface vs flux $r^2/2$ at the midplane of the central cell with B normalized to unity: (a) TMX-B: $\beta_c = 0.35$, $\beta_p = 0.35$; (b) MFTF-B: $\beta_c = 0.15$, $\beta_p = 0.35$.

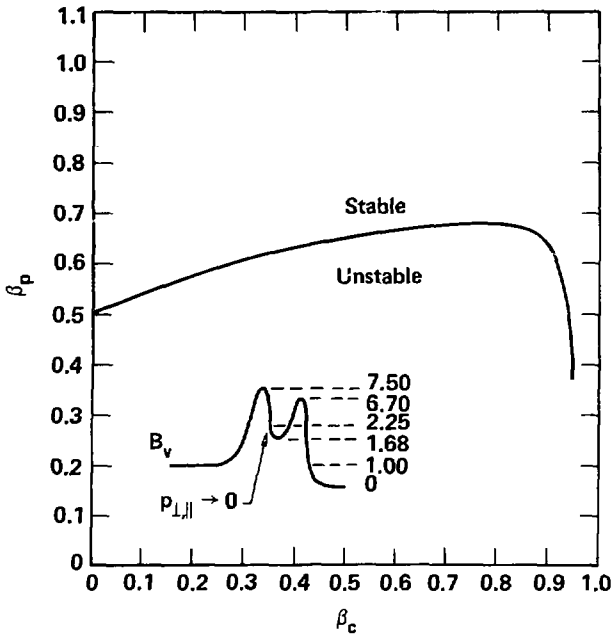

FIG. 2. Beta stability diagram for a wall-stabilized, axisymmetric tandem mirror with $s_\beta = (R_w/R_p - 1)/2 = 0.2$ and $L_p << L_B$.

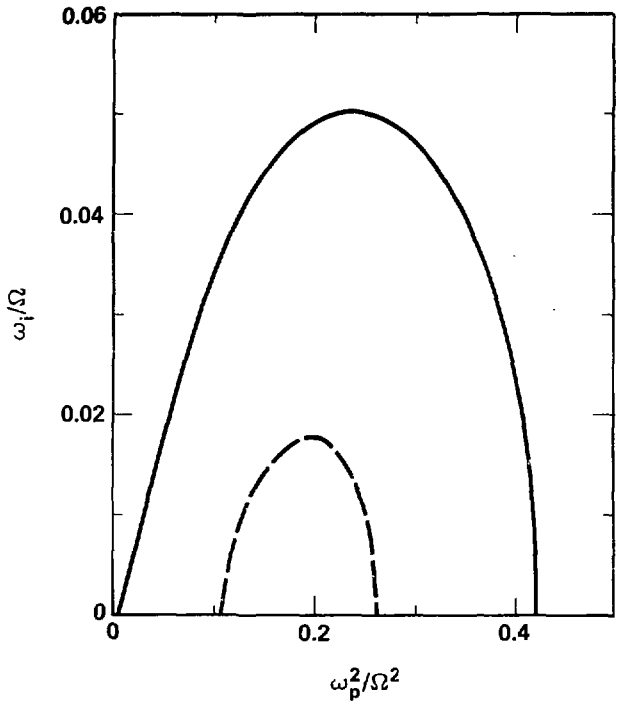

FIG. 3. Growth rate of cyclotron-maser instability at $\vec{k} = 0$ as a function of density. The two curves contrast the results obtained with two different energy distributions. Parameters are $E/mc^2 = 0.15$, $\theta = 60^o$, and $n_{cold} = 0$.

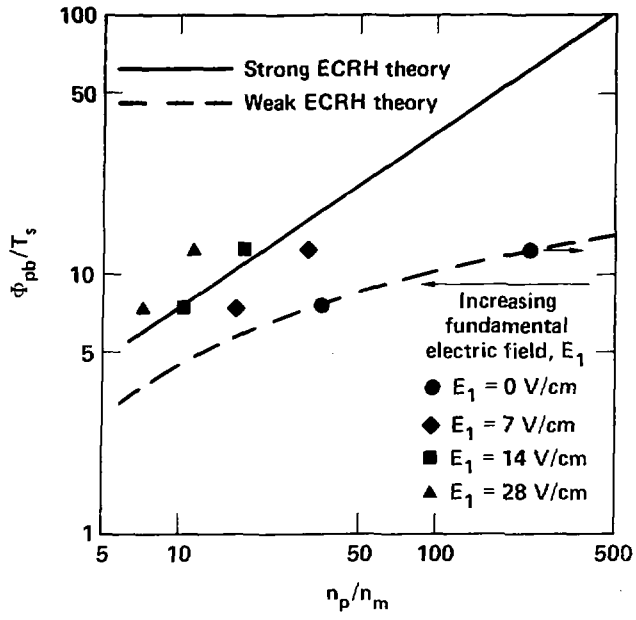

FIG. 4. Potential between the thermal barrier and end plug vs plug density. Data points are Fokker-Planck code results showing the transition from the weak to strong ECRH regimes.